공학석사학위논문

Design improvements of the Smart Active Trailing-edge Flap (ATF) for Rotating Test

헬리콥터 진동제어용 지능형 능동뒷전 플랩의 회전시험을 위한 설계의 개선

2015년 2월

서울대학교 대학원

기계항공공학부

강정표

Design improvements of the Smart Active Trailing-edge Flap (ATF) for Rotating Test

헬리콥터 진동제어용 지능형 능동뒷전 플랩의 회전시험을 위한 설계의 개선

지도교수 신 상 준

이 논문을 공학석사 학위논문으로 제출함

2015년 2월

서울대학교 대학원
기계항공공학부
강 정 표

강정표의 석사학위논문을 인준함

2015년 2월

위 원 장 李栽甲 (인)

부 위 원 장 申尙埈 (인)

위 원 李晉中 (인)

Abstract

In this dissertation, small-scaled blade prototypes with the flap-driving mechanism, called SNUF (Seoul National University Flap), were manufactured, and tested in order to realize vibratory load reduction in the rotor system. It was achieved by an active trailing-edge flap which is based on piezoelectric actuator. However, it turned out that the target value (±4°) of the flap deflection angle was not accomplished in the previous designs. Therefore, the flap driving mechanism needs to be amended. Thus, a new piezoelectric actuator was selected to achieve the target deflection by considering the nonlinear relationship between flap deflection angle and the moment arm length. Re-selection of the actuator required increase of the blade inner space and its size. Therefore, it was required to validate the cross-sectional design of the improved blade configuration. So as to verify the structural integrity, cross-sectional analysis was conducted by using UM/VABS. Revised flap driving mechanism and its test-bed shows quite satisfactory result during the static bench test even though there still remain several issues which should be solved. After completion of the non-rotating static test of the new flap-driving mechanism, a prototype blade will be manufactured and tested in the whirl tower.

Keywords: Active Trailing-edge Flap (ATF), piezoelectric actuator, vibration control, active rotor blade

Student Number: 2013-22481

Table of contents

List of Figures

List of Tables

I. INTRODUCTION

1.1 Backgrounds and motivation

Helicopters have carried out a crucial role in modern aviation industry with capabilities based on the distinctive hovering, vertical take-off and landing. These unique advantages enable helicopters to conduct multiple roles in both civilian and military operations such as air medical services, firefighting, vertical replenishment. However, helicopters are inherently involved with the noise and vibration as a result of intrinsic aerodynamic imbalance in the rotor system, as shown in Figure 1.1, such as the flow speed difference between the advancing and the retreating blade, and the helical tip vortex (also called BVI : Blade Vortex Interaction) which the all blades generate.

Vibration in helicopters is still an unresolved issue which poses numerous challenges, especially when passenger comfort is concerned; the highly asymmetric aerodynamics encountered during both forward flight and descent generates acoustic noise and vibration which result in an unfriendly environment. This vibration is also responsible for reduction in component service life as well as degradation in structural integrity. Consequently, various vibration reduction methods have been introduced so as to obtain a better crew comfort, increase components service life.

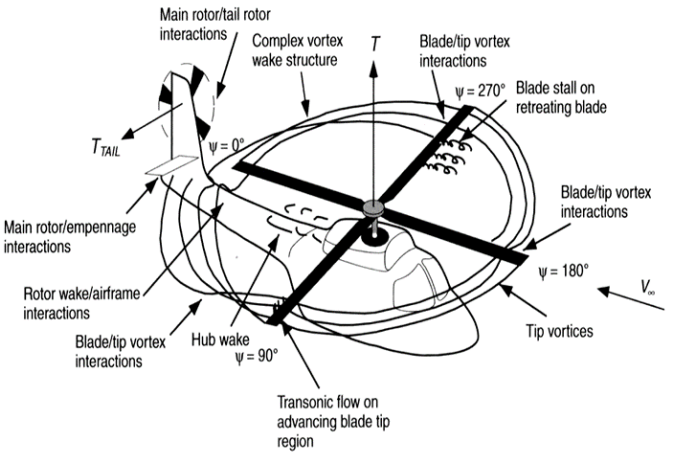

Figure 1.1 Aerodynamic problems during forward flight

1.2 Vibration reduction methods

The conventional vibration reduction method was passive. Passive methods have been applied so far, whose goal was to adsorb vibrations from its transmission to the fuselage. The most widespread methods are bifilar absorbers as shown in Figure. 1.2, placed between the main rotor and the fuselage, or hydraulic control systems which generate vibrations on the fuselage aiming at eliminating the primary vibratory loads. The methods mentioned above, along with a noticeable increase in overall weight, are not capable of promptly responding to changes in flight conditions [2]

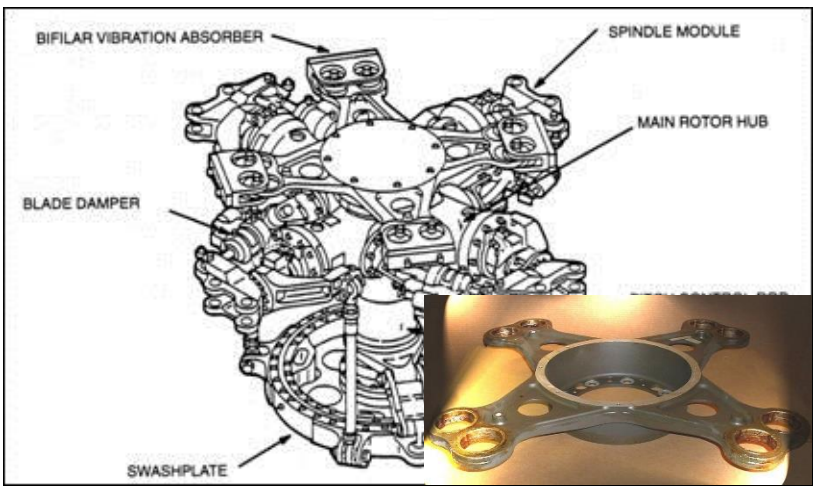

Figure 1.2 UH-60 Blackhawk bifilar vibration absorber

As a matter of fact, loads which spring from the main rotor are characterized by pN/rev harmonics where N is the blade number and p an integer, are not cancelled out [1]; conventional control systems which use swashplate and pitch link are unable to cope with such phenomena due to their constraint to 1/rev frequency. However, active control methods display higher adaptability to the flight environment as well as increased results in the vibrations reduction [3]. Consequently, active control methods have attracted the attention of many researchers, and helicopter industries. In recent days, it has become main stream of helicopter vibration reduction methods. Active vibration methods could be categorized into following two groups;

1. Aimed to attenuate the vibration in the fuselage

2. Aimed to alleviate the vibration on the rotor before it reach in the fuselage.

First, Active Control of Structural Response (ACSR) aims to attenuate the vibration in the fuselage directly. This ASCR scheme is based on the idea that in a linear system one can superimpose two independent response quantities such that the total response is zero [4]. This scheme also shows satisfactory results of vibration reduction, and it is used on production helicopter such as EC225 as shown in Figure 1.3, EH101, Sikorsky S76, etc. The schematic diagram how the ASCR operates is denoted in Figure 1. 4

Figure 1.3 EC225's AVCS (Anti-vibration control system) using the ASCR active control method.

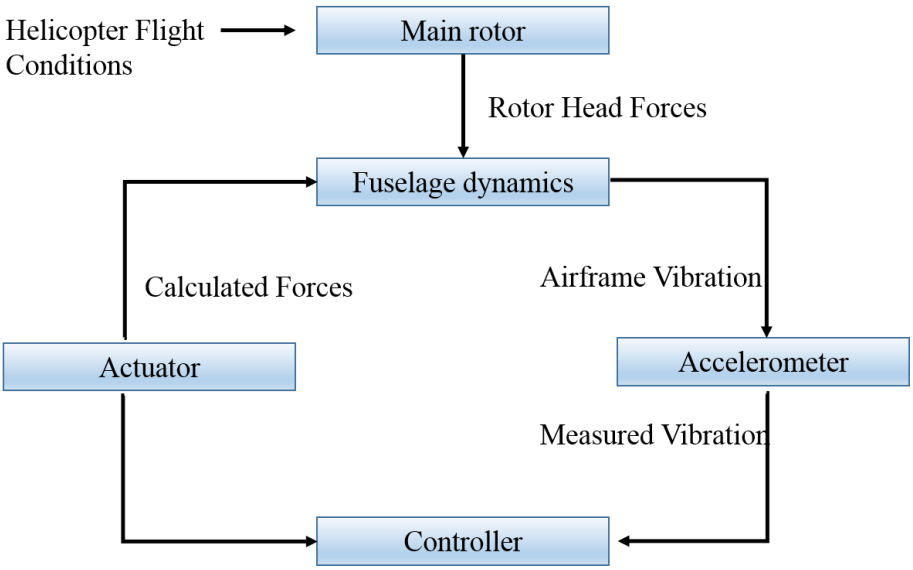

Figure 1.4 Schematic diagram for ASCR

The second category of active control approach aims to alleviate vibration in the rotor directly, not in the fuselage. This methods could be fallen into two types. First type, Higher Harmonic Control (HHC) is that the blades are activated in the nonrotating swashplate by introducing pitch commands [5]. The purpose of this vibration reduction method is to engender higher harmonic unsteady aerodynamic loads on the rotor blades that cancel the original loads accountable for the vibration. Despite this HHC method demonstrated successful vibration reduction results compared to the passive methods, there are still challenging problems existing. Both weight penalty of the heavy actuator and high actuation power are still problems which should be resolved. However, the principal drawback is the limitation to certain control frequencies ($kN_b \pm 1$)/rev, and due to the fact that noise and vibrations could often not be reduced at the same time [6]. In

attempt to overcome this limitation of HHC, Individual Blade Control (IBC), where each blade can be controlled independently in the rotating frame, seems the most promising alternatives in present days. Many IBC technologies have been designed, manufactured, and tested. The major implementation cases of IBC technology are as follows.

1. The earliest implementation depicted in Figure 1.5 , based on pitch actuation at the blade root(off-blade actuation) in the rotating system, replaced the conventional control rods which was connected the swashplate with active actuators.

2. The Active-Twist Rotor (ATR) where the entire blade is twisted along the blade span (on-blade actuation) as shown in Figure 1.6. It normally uses the piezoelectric fibers embedded in the blade.

3. The actively controlled partial-span trailing-edge flaps (on-blade actuation), or called Active Controlled trailing-edge flaps (ACF) depicted in Figure 1.7.

ATR has shown good vibration reduction results by twisting the whole blade along the span. However, it needs high input voltage (larger than 2,000volts) to enable the linear twist of the ATR blade for enough vibration alleviation. That is one of the reasons why ACF concept emerged. ACF does not need high input voltage to operate the piezoelectric actuators which enable the vibration alleviation. Furthermore, ACF has also shown effective vibration reduction level by altering aerodynamics of the blade like ATR does. Thus, this dissertation will be limited to consideration of ACF concept as exploring the question of the vibration reduction.

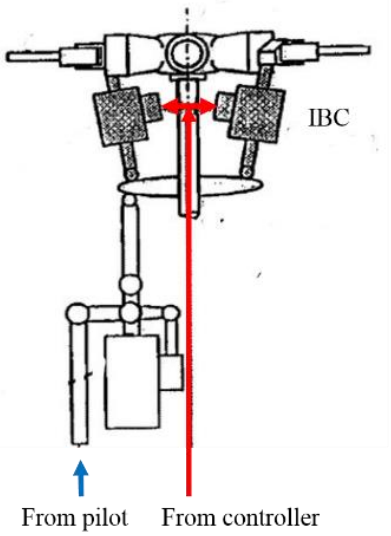

Figure 1.5 Individual blade control

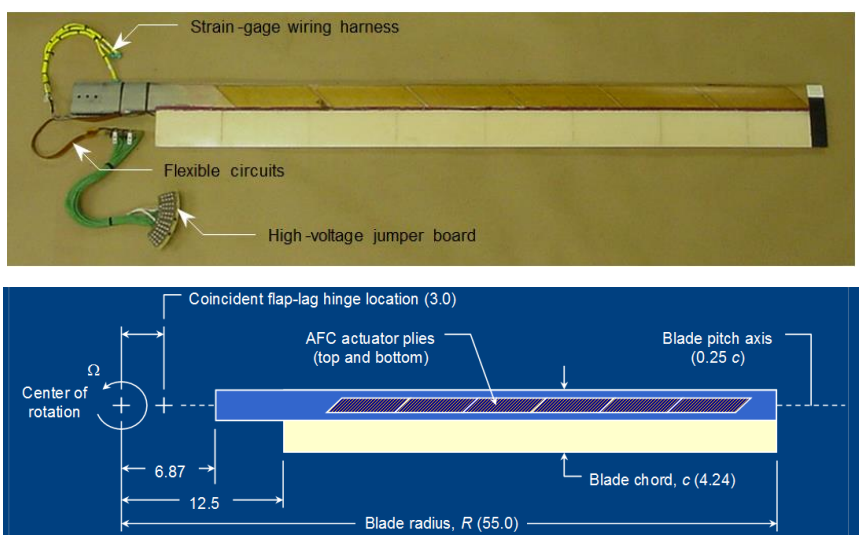

Figure 1.6 ATR blade (NASA/ARMY/M.I.T.)

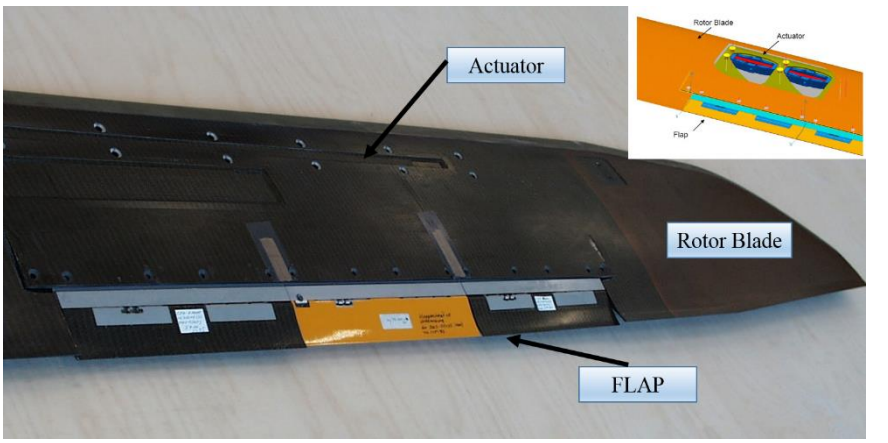

Figure 1.7 Active partial-span trailing-edge flaps of Eurocopter BK117.

1.3 Previous related researches

There is no dispute that ACF (Active Controlled trailing-edge Flap) concept on-blade vibration reduction method is one of a state-of-the art IBC technology. Aforementioned above, there are several related researches about on-blade actuation mechanism of based on piezoelectric actuator. Two notable examples of ACF concept based on utilizing smart material actuators are as follows. First, ABC (Active Blade Concept), a four bladed Mach-scaled rotor as shown in Figure 1.8, was manufactured by the cooperation of DLR, ONERA, and Eurocopter Deutschland. The APA 500 piezoelectric actuator, depicted in Figure 1.9, manufactured by the French Cedrat company was used to enable the flap deflection of the ABC. Wind tunnel test for the interests related to aerodynamics, acoustics and dynamics were conducted in 2005[7]. As shown in Figure 1.10, ATE (Active Trailing-

Edge) blade manufactured by Eurocopter is an integrated active trailing edge concept. It consists of the cut-out blade and the actuator unit with the active flap. The cut-out blade trailing section is filled with the several segments of the housing inside which the actuator is installed. Those individual segments were designed to reduce the normal strains. This modification makes it possible to use the piezo-ceramic materials as bending actuators at the trailing edge [8]. The worldwide official first flight of a helicopter with active trailing edge flaps took place in 2005, as depicted in Figure 1.11. The subsequent intensive flight test showed excellent results in terms of system performance as well as endurance. Relevant noise and vibration control tests were performed successfully [9].

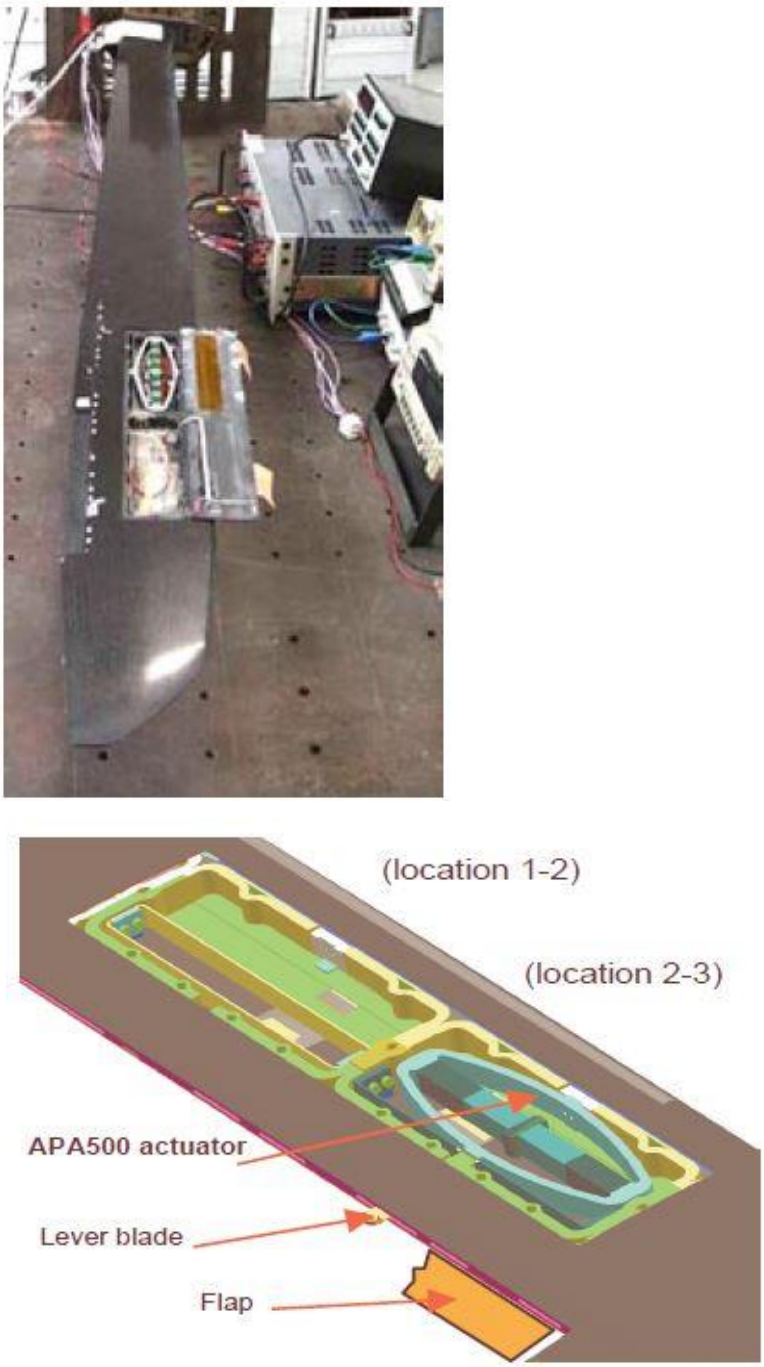

Figure 1.8 Active Blade Concept rotor and actuation parts.

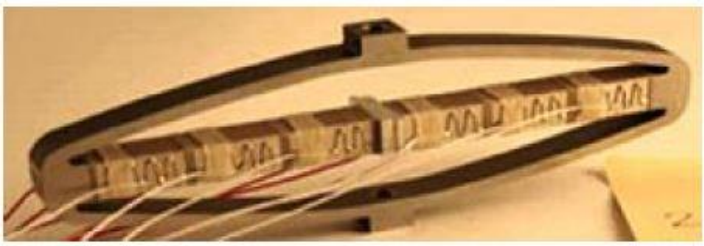

Figure 1.9 APA 500L piezoelectric actuator.

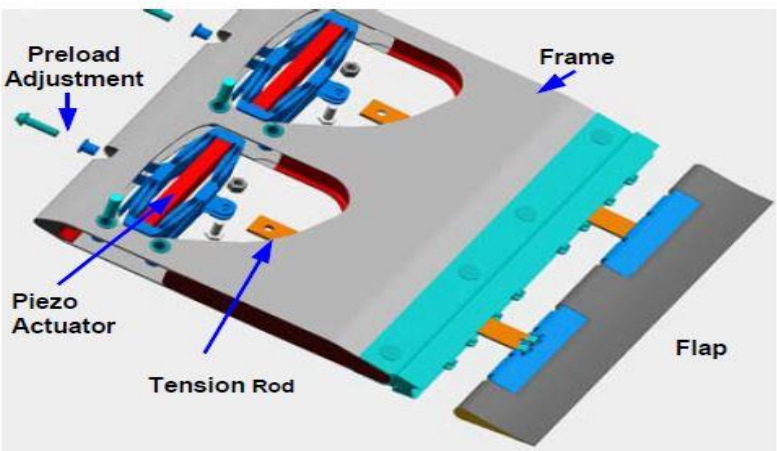

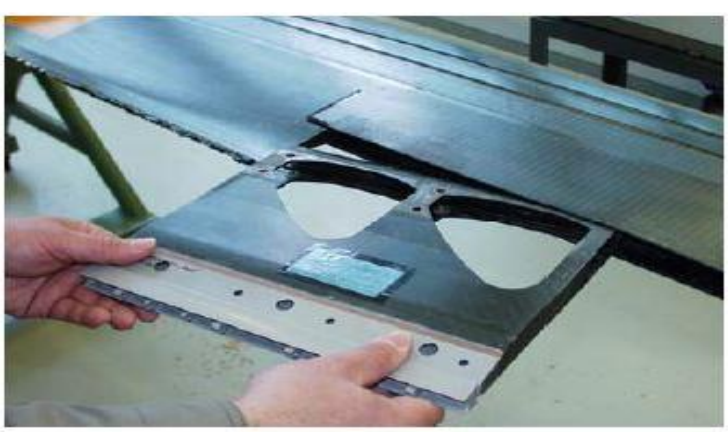

Figure 1.10 Integration of flap modules into the rotor blade structure at the trailing edge for ATE

Figure 1.11 First flight of a BK 117 with Active Trailing-edge Flaps

1.4 Objectives and Overview of the dissertation

The present helicopter design technologies have not yet been able to completely eliminate the high levels of noises and vibrations. These problems are still unsettled, even though several research projects have been kicked off in order to develop advanced rotor control systems to address those matters. However, the smart material of the current day made it possible that the piezoelectric actuators become light-weighted, compact and low power requirement. It also allows to prevent the actuator mechanism become complicated to manufacture. In line with this development of the smart material, the small-scaled blade prototypes with the flap-driving mechanism, called SNUF which based on the smart material (piezoelectric actuator), were manufactured, and tested in order to realize vibratory load reduction in the rotor system by the previous researcher. However, it turned out that the target value (±4°) of the flap deflection angle

was not accomplished in the previous designs. Therefore, the flap driving mechanism needs to be amended. As a result, this dissertation has the objective to improve the design of the previous SNUF (Seoul National University Flap) which uses the ATF(Active Trailing-edge Flap) method in order to attenuate noises and vibrations of an helicopter. SNUF blade design improvement processes in this dissertation were divided into the following three categories.

1. The new piezoelectric actuator selection process
2. Flap-driving mechanism revision
3. Blade structural design and analysis for the revised SNUF

The new piezoelectric actuator selection process ran parallel with the aerodynamic hinge moment analysis in order to achieve the target value. Commercial CFD program Fluent was used for the aerodynamic hinge moment of the flap. Flap-driving mechanism revision process was carried out after the selection of the new actuator so as to obtain the required flap deflection angle. Several static bench tests were conducted to get the feedback and to apply the necessary amendments for achieving the desired flap deflection. The blade structural design and analysis process was carried out for the revised SNUF. So as to verify the structural integrity, a cross-sectional analysis was conducted by using UM/VABS, and CAMRAD II.

The scope of this thesis is limited from the actuator reselection, flap-driving mechanism revision with static bench test, and structural integrity analysis. However, the ultimate goals of this research are to manufacture the SNUF blade test-bed, to design higher harmonic control system, and to conduct the whirl tower test to verify dynamic characteristics.

II. Flap-driving region revision and tests

2.1 Previous works review

Static bench test is an initial step for validating flap mechanism before testing in the actual force fields like aerodynamic and centrifugal ones. However, the previous models of SNUF could not achieve the desired flap deflection during the static bench test [10]. It is mainly assumed that the unexplained friction force arose more than it was expected to occur. Table 2. 1 indicates the results of the bench tests. After the bench test of the first flap driving mechanism model, which is depicted in Figure 2.1, failed, the method coping with the failure was revision of the flap driving mechanism design with the increasing number of actuators one by one until the target flap deflection is achieved. It turned out that this method was not effective for attaining the target value. Accumulating actuators one by one shown in Figure 2.1 (version 4) could not convert the linear motion into rotary motion without any loss of the force. It is observed that unpredictable friction force occurred between two actuators, and slight misalignment might reduce the capability of the actuators. What it proves to us that the method mere adding the actuators could not be an effective way to solve the problem. It probably attains the satisfactory static bench test results in the end if the unlimited number of actuators can be installed to deflect the flap. Inasmuch as the inner space for the actuators is limited, this method is unreasonable. There are also increasing concerns about weight penalty as increasing number of the actuators. Based on these disadvantages, the APA 200 piezoelectric actuator using on the flap driving region was abandoned. Thus, this project needs to be started from scratch by the sequence of the design flowchart as

shown in Figure 2.2.

Table 2.1 Results of the previous configuration [9]

Version	Configuration	Flap Deflection
1	Single actuator – Skin hinge type	± 2°
2	Two actuators in parallel – Pin hinge type	± 1.5°
3	Three actuators in parallel – Pin hinge type	± 2.5°
4	Four actuators in parallel and series – Pin hinge type	± 3.7°

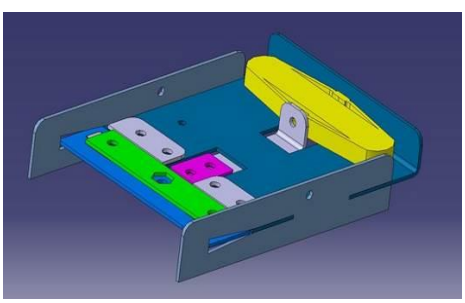

(a) Version 1

(b) Version 2

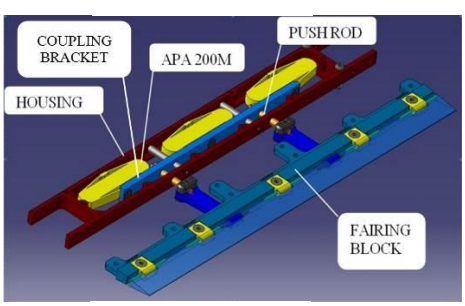

(c) Version 3

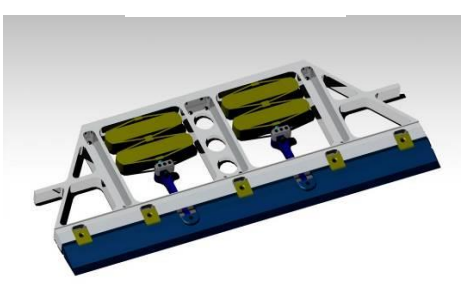

(d) Version 4

Figure 2.1 Previous driving mechanism configurations

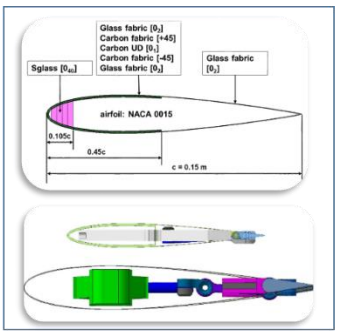

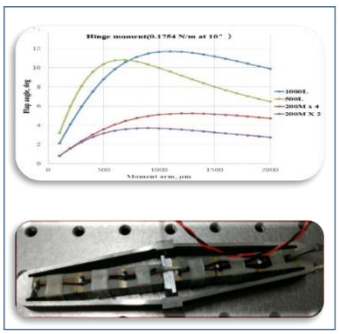

Blade cross sectional design,
Structural analysis

Aerodynamic analysis by Fluent
Actuator selection

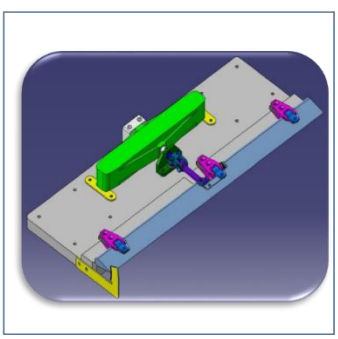

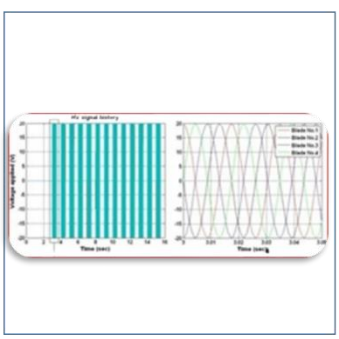

Flap driving mechanism design

Control algorithm design

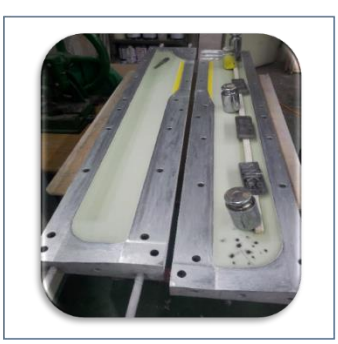

Manufacturing Test-bed blade static bench & Rotational test

Figure 2.2 Design flowchart

As a first step to solve the problems in the previous design, the actuator reselection step was conducted before the structural analysis of the blade configuration was attempted. In the past the blade structural analysis was done at first, then the appropriate piezoelectric actuator which can be inserted in the inner space of the blade was selected. In other words, the pre-designed blade configuration factors such as length, thickness and twist distribution caused the limitation of actuator model selection. The limited inner space forced to use a small actuator. The only alternative ways to achieve the target value was accumulating the actuators one by one in order to produce more force to deflect the flap until the target value was to be achieved. However, it ended in failure. Consequently, those alternative measures not only increased the complexity of the flap driving mechanism, but also reduced the capability of the actuator to deflect the flap. Therefore, fundamental revision steps including reselection process for the actuator which can overcome the hinge moment acting on the Active Trailing-edge Flap were needed in advance. In accordance with this principle, actuator selection process was carried out, regardless of inner space size of the blade. In the following section, the prediction of the hinge moment procedure will be introduced as the first step to obtain the target value. The limited inner space brought about problems regarding to actual manufacturing simplicity and the size of the piezoelectric actuator. As the smaller inner space for actuator, the bigger and the stronger actuator cannot be used SNUF blade based on the design of the existing NASA/ARMY/MIT Active Twist Rotor (ATR) blades [13] and SHARCS [14]. They were all small scaled rotors. Consequently, the previous SNUF blade model's piezoelectric actuator selection was limited by the blade design with the small inner space.

2.2 Prediction of hinge moments

In order to achieve the target value of ATF deflection (±4°) in the rotating environment, designing the effective linkage mechanism is imperative. In addition, the estimation of the flap hinge moments will be crucial factor in order to select the optimum actuator which can overcome aerodynamic force on the flap. The aerodynamic hinge moment prediction was done by using Computational Fluid Dynamics FLUENT program. Before applying this FLUENT program, it is needed to show the credibility of modeling for ATF. Therefore, verification procedure was implemented with the comparison of the NACA 4415 at several angles of attack. As shown in Figures 2.3 and 2.4, it showed quite well agreed results except for a little of spikes. Thus, aerodynamic analysis on SNUF was conducted using this modeling method which is shown in Figure 2.5. The aerodynamic analysis conditions are shown in Table 2.2, and Table 2.3 indicated the results. The flap hinge moment value at AOA 10° was the largest value.

Another aerodynamic hinge moment prediction by adopting the formulas suggested by Lee [12] was also carried out for comparison with CFD FLUENT results. 0.2727 N-m at an angle of attack at 10° was the maximum value from Equation (1). The hinge moment comparison results are shown in Figure 2.6. In general, the CFD FLUENT analysis results were obtained to be 20% higher than that predicted by the formula proposed by Lee. Therefore, CFD FLUENT analysis results were adopted for more conservative approach. The maximum value at an angle of attack at 10° was 0.3249 N/m from the CFD FLUENT. Therefore, this value was chosen as the critical hinge moment value.

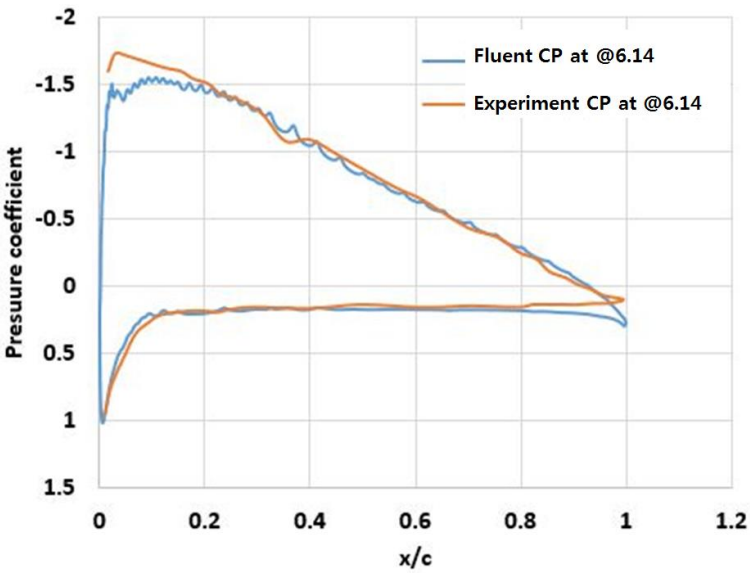

Figure 2. 3 Pressure coefficient at Cp at AOA 6.14˚

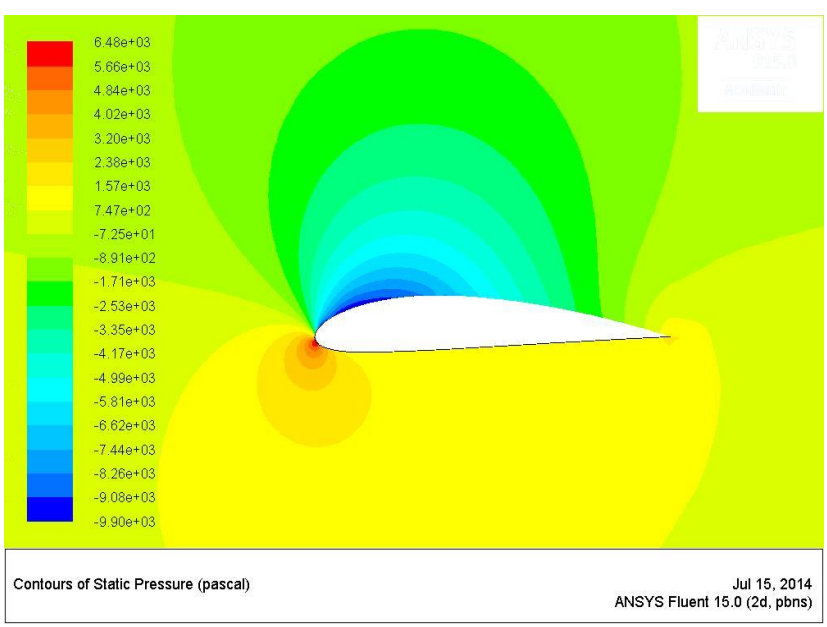

Figure 2. 4 Static Pressure distribution at AOA 6.14˚

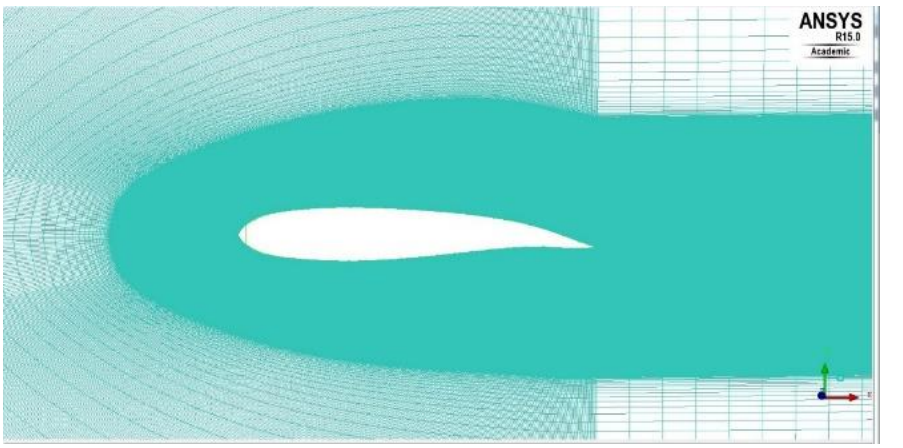

Figure 2. 5 NACA 0015 FLUENT analysis with a trailing edge deflected by 10°

Table 2. 2 The SNUF aerodynamic analysis conditions

Flap location	75% R [1.125 m]
Flap length	20% R [0.3 m]
Flap chord	15% C [0.203m]
V(advancing side)	156.1879 m/s
Mach number	0.45
Flap deflection(δ)	10°
Fluid density	1.1767 kg/m3
Temperature	300 K
Flow condition	Compressible, inviscid

Table 2. 3 The SNUF aerodynamic analysis results

α(°)	Lift coefficient	Flap hinge moment coefficient	Flap hinge moment (N·m)
0	0.3722	0.00816	0.3204
3	0.5355	0.00792	0.3108
7	0.7639	0.00836	0.3282
10	0.8314	0.00828	0.3249

$$H = \frac{1}{2}\rho\Omega^2 c^2{}_f \left[\left(\frac{R_2^{\,3}}{3} - \frac{R_1^{\,3}}{3}\right) \times \left\{C_{l_\alpha} \frac{dC_h}{dC_l}\left(\theta + \frac{\Delta\alpha_{eff}}{\Delta\delta}\delta\right) + \frac{dC_h}{d\delta}\delta\right\}\right.$$
$$\left. - C_{l_\alpha}\lambda R_{tip}\left(\frac{R_2^{\,2}}{2} - \frac{R_1^{\,2}}{2}\right)\frac{dC_h}{C_l}\right] \qquad (1)$$

ρ : the air density, Ω : the rotor rotational speed

c_f : the flap chord, R_1 / R_2 : the inboard/outboard flap location

θ: the blade collective pitch, λ: the rotor inflow

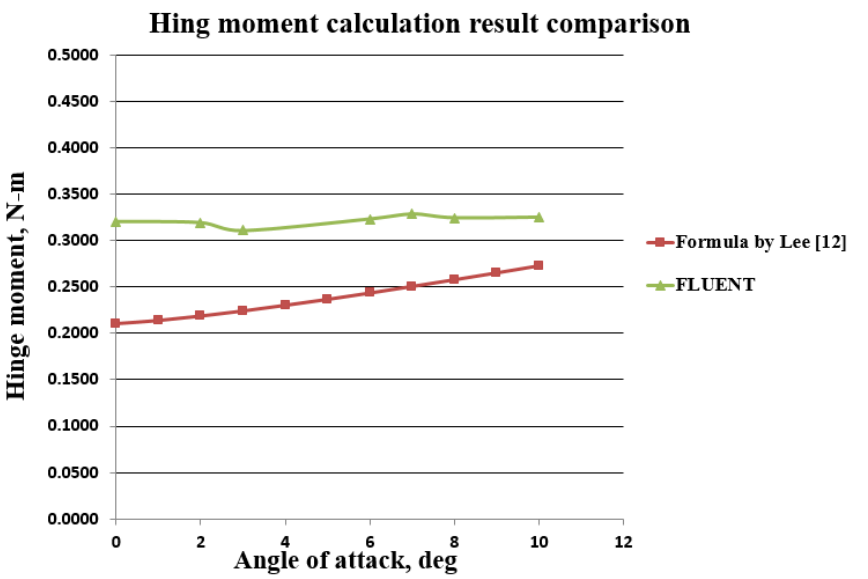

Figure 2. 6 Hinge moment comparison results

2.3 Reselection of the actuator

Because the actuator of ATF should be able to do higher harmonic motions, it needs rapid response capability. Based on this criterion, the piezoelectric actuators have been used widely for the active rotor control. In the previous research on SNUF, the APA 200M actuator was selected in the light of the SNUF inner space and its size. However, the block force of a single actuator was not sufficient to activate the flap. Therefore, multiple actuators were considered to enable the required flap deflection. The test was carried out by increasing the number of 200M actuators from one to four actuators. However, the results were not satisfactory. One of the speculative reasons was the increasing number of the actuators ensue the complication of the actuation region. It is for granted that the complicated flap-driving mechanism was not effective to deflect the flap due to occurrence of the uncertain amount of the friction force. In addition, the moment arm length (L_2), which converts the linear motion of the actuator into rotary motion, became smaller since the limited displacement range of the APA 200M actuator. This factor led to the discrepancies from the estimated flap deflection angles. Consequently, so as to obtain the desired flap deflection angle, several actuators in Table 2.4 were reconsidered regardless of its size and mass, but with regard to the available block force and displacement range. The force and displacement relations of actuator are depicted in Figure 2.7.

Table 2. 4 Standard properties of various APA actuators

Properties	200 M	500 L	1000 L
Max.no load displacement (µm)	230	500	900
Blocked force (N)	73	570	373
Force limit (0-pk) (N)	27.38	285	93.25
Height (mm)	17	55	35
Length (mm)	55	145	145
Width (mm)	9	16	16
Mass (g)	15.7	200	190

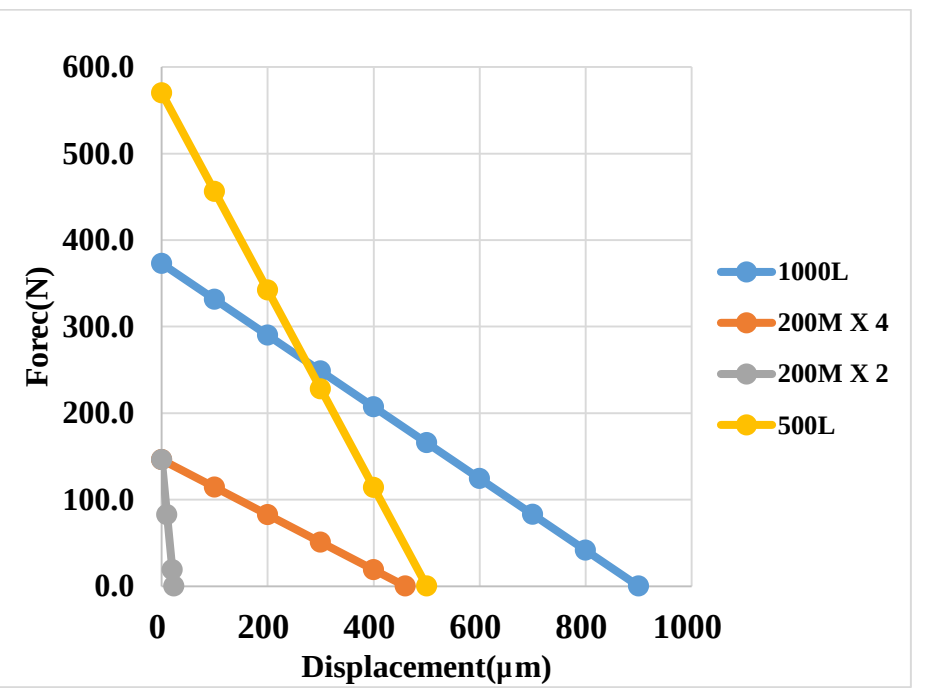

Figure 2. 7 Force and displacement relations

First of all, an appropriate length of the moment arm (L_2), shown in Figure 2.8, needed to be re-estimated in order to find that relations between the force and the displacement for the candidate actuator models. Previous APA 200M actuator's free/maximum stroke was 0.23mm, according to the specification in Table 2.4. As a result of the low stroke capability, the moment arm (L_2) length has constraint on its length, which led to unsatisfactory results in the end.

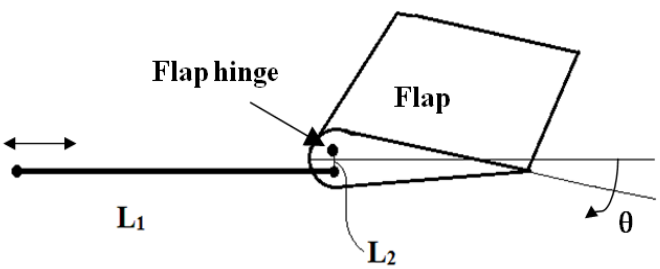

Figure 2.8 Schematic of the linkage mechanism

Figure 2.9 shows an angle deflection range of the candidate actuator product, and the available moment arm length range. The APA 1000L actuator shows wider flap deflection angle range and longer moment arm available range above the specific target value (±4°). Furthermore, according to Mainz [15], the flap deflection angle was decreased about 30~50% at the non-rotating aerodynamic test in the wind tunnel. It seems reasonable to assume that flap deflection angle should be larger than ±8° in the non-rotating static bench test to achieve the target value. Making allowance for this fact, APA 1000L actuator with enough the block force was selected to withstand the aerodynamic force acting on the flap.

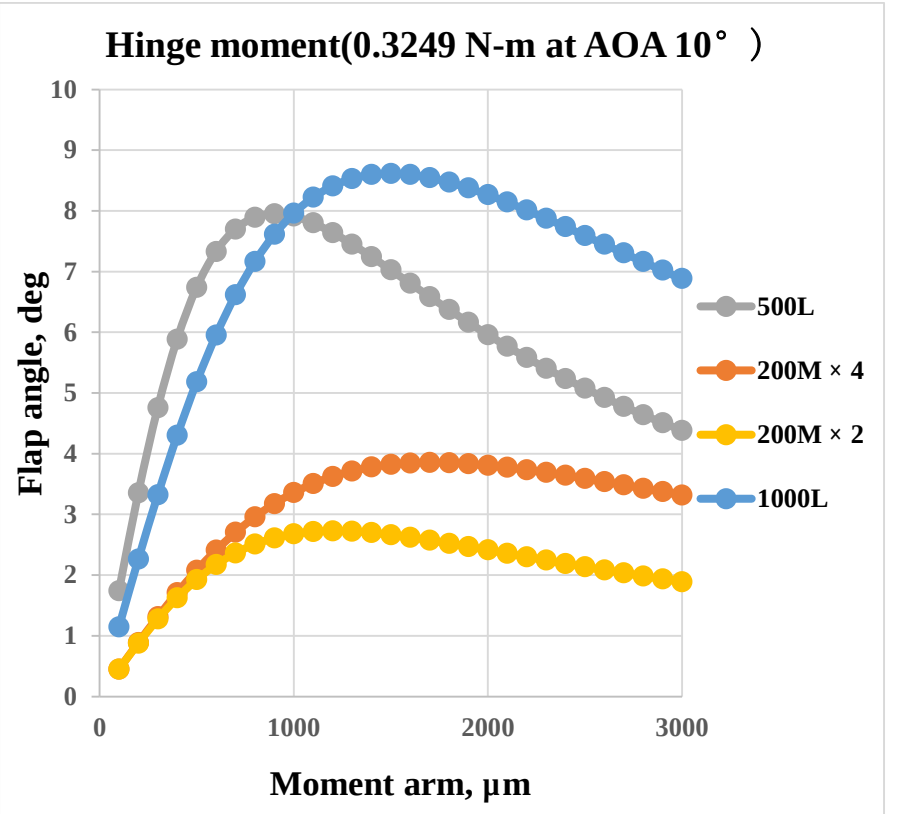

Figure 2. 9 Flap deflection and moment arm length relationship

2.4 Static load analysis for the actuator

In this thesis, the rotor RPM to be considered was quite high to achieve the required tip Mach number at the blade tip. It induced a large centrifugal force on the actuator. At the actuator, the centrifugal force and piezoelectric force were applied. Therefore, static load analysis was required to validate its structural safety. To implement piezo-structural analysis by the commercial finite element analysis program, MSC. NASTRAN, a simple thermal analogy was employed. The piezoelectric strain generated by an electric field was equated to the thermal strain generated by an equivalent temperature change. The APA1000L had six piezo-stacks, and an electric field was applied to each piezo-stack, as shown in Figure 2.10.

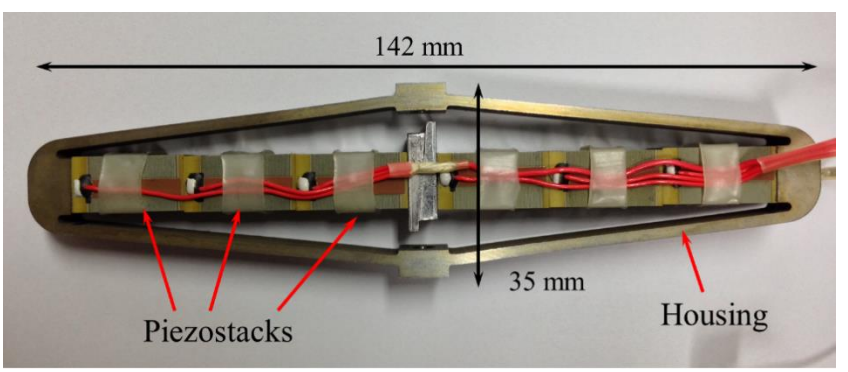

Figure 2. 10 APA1000L actuator

The total piezoelectric strain of APA1000L generated by an electric field is expressed in Eq. (2). Using this equation, equivalent thermal expansion coefficient and equivalent temperature were obtained as follows.

$$\varepsilon^{piezo} = 6 \times d_{33} \Phi = 6 d_{33} \frac{V}{t} \tag{2}$$

$$\varepsilon^{thermal} = \alpha_{eq} \Delta T_{eq} \tag{3}$$

$$\alpha_{eq} = \frac{6 d_{33}}{t}, \quad \Delta T_{eq} = V \tag{4}$$

where, d_{33} is the longitudinal piezoelectric coupling coefficient, t is thickness of piezo-stack, and V is voltage, applied to piezo-stack. The specific properties for the thermal analogy analysis are summarized in Table. 2.5.

Table 2.5 Properties used in the present thermal analogy

d_{33} [m/V]	t [m]	V [V]	α_{eq} [℃-1]	ΔT_{eq} [℃]
2.75 x 10-10	18 x 10-3	150	9.17 x 10-8	150

Static load analysis was performed under three different load cases: only centrifugal force, only piezoelectric force by thermal analogy, and total load case. For each case, the strain of APA1000L was predicted by using MSC. NASTRAN. The stainless steel material properties were used for the housing component. To apply the centrifugal force, the rotation speed was 21.08 rad/s, and the distance between rotational center and actuator was 1.125 m. The equivalent thermal expansion coefficient and temperature rise of 150℃ were applied to the piezo-stack region. The results of strain distributions are shown in Figure 2.11.

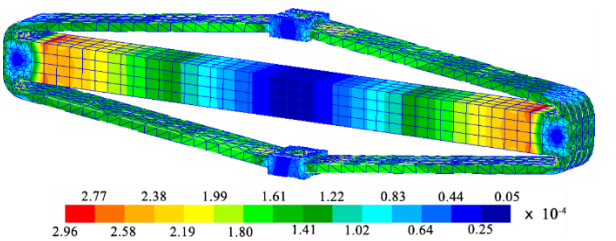

(a) only centrifugal loads

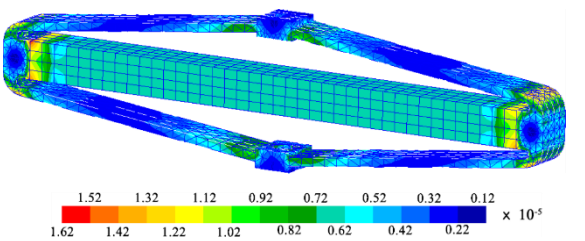

(b) only piezoelectric actuation

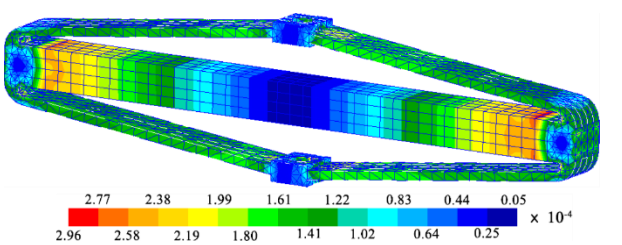

(c) centrifugal loads + piezoelectric actuation

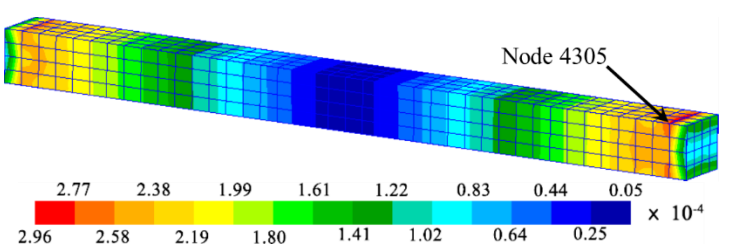

(d) piezo-stack component under the combined loads

Figure 2. 11 Von Mises strain distribution under the static loads

The strain value at the node 4305, as shown in Figure 2.11 (d), which had the maximum von Mises strain value under the total force application, was compared and it is summarized in Table 2.6. The strains under the total force were the summation of each strain value obtained from centrifugal force and piezoelectric force. Through this procedure, the structural validity of APA1000L was authenticated.

Table 2.6 Strains (με) induced in Node 4305

Applied force	Longitudinal Strain(με)	Lateral Strain(με)	Transverse Strain(με)	Allowable Strain(με)	Maximum /Allowable
Centrifugal force	-268	81.3	103	800	33.5 %
Piezoelectric force	2.35	2.74	2.68	800	0.34%
Total force	-265	8.4	109	800	33.1%

2.5 Revision of the flap-driving mechanism

It is extremely important to design the efficient linkage mechanism in order to obtain the target value. However, as mentioned before, the previous design shown in Figure 2.12 was not capable of achieving the desired target value, and the results are depicted in Table 2.7. It was because of the un-estimated friction force, and the increased complexity of the flap-driving mechanism. Therefore, comprehensive amendments have been implemented, including improving the actuator product and simplifying the linkage mechanism to prevent loss of the block force.

Table 2. 7 Results of the previous configuration [10]

Version	Configuration	Flap Deflection
(a)	Single actuator – Skin hinge type	± 2°
(b)	Two actuators in parallel – Pin hinge type	± 1.5°
(c)	Three actuators in parallel – Pin hinge type	± 2.5°
(d)	Four actuators in parallel and series – Pin hinge type	± 3.7°

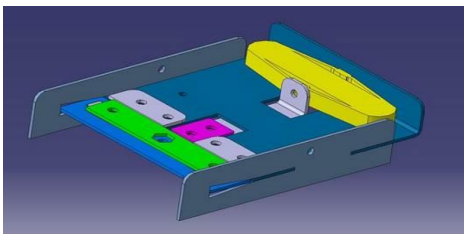

(a) Single actuator

(b) Two actuators in parallel

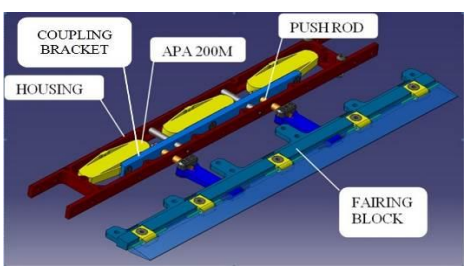

(c) Three actuators in parallel

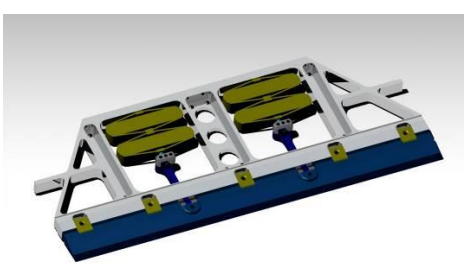

(d) Four actuators in parallel and series

Figure 2. 12 Previous flap driving mechanisms by using APA 200 M actuator

As a result of estimating the flap deflection angle and moment arm length relationship, APA 1000L showed an optimistic operational condition for the present ATF. Later, appropriate length of the moment arm (L_2) will be determined by multiple iterative operations, which examines the nonlinear relationship between the flap deflection angle and the moment arm length, through the new test-bed design depicted in Figure 2.13.

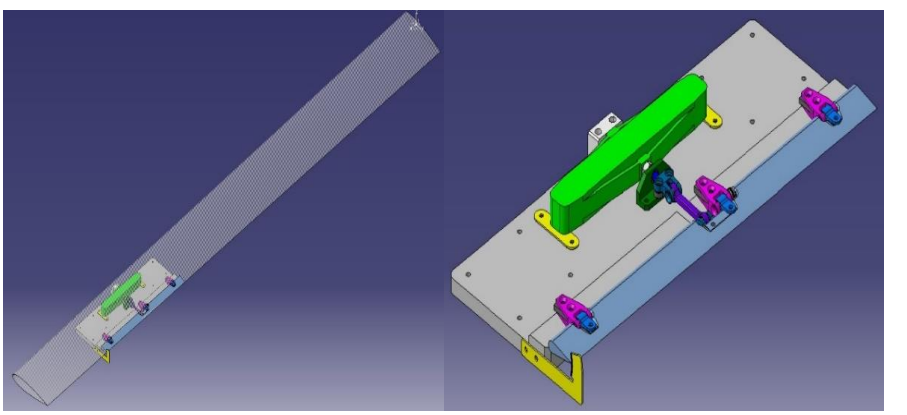

Figure 2.13 New APA 1000L actuator test-bed

Though its whole mass was increased due to increments of the width and length, the newly designed APA 1000L actuator test-bed design reduced the complexity of the actuation region as well as increased the block force and the available moment arm length. As a result, simple linkage mechanism shows increased possibility of achieving the target deflection of the flap during the rotational dynamic test. As a result, current non-rotating test for the new flap driving mechanism showed around 20°at 10 Hz actuation frequency of the actuator. Another advantage of the revised flap – driving mechanism is that the bigger moment arm (L_2) length provides further convenience on manufacturing of the hinge pin offset part (L_2 part).

Lastly, thrust bearing, shown in Figure 2. 14, was added along the flap axis to prevent axial direction loads caused by centrifugal force. Considering the hinge shaft diameter (3mm), F3-8M thrust bearing was one of the most suitable miniature bearings to be installed in the present active flap. In addition, magnitude of centrifugal loads acting on the active flap is required to be lower than the load rating of the thrust bearing. The flap is estimated to weigh 29 g and it results in centrifugal force of 603N for 1,303 RPM at 75 % span of the rotor radius 1.5 m. Thrust bearing F3-8M has a static load rating of 590N and a dynamic load rating of 993N. Consequently, the centrifugal force acting on the present active flap fell into acceptable thrust load rating. In spite of several advantages of the newly designed APA 1000L actuator test-bed, it was inevitable to enlarge the blade length and thickness in order to accommodate the revised APA 1000L actuator into the inner space of the blade. Therefore re-analysis of the structural integrity was required for the revised blade design. Detailed analysis results will be included in the next chapter in Blade design and analysis. The differences of two blades were summarized in Table 2.8.

Table 2.8. Revised SNUF properties

Specs.	Previous SNUF	Present SNUF
Rotor radius (cm)	128	150
Rotation speed (rpm)	1,528 (160 rad/s)	1,303 (136 rad/s)
Blade chord (cm)	10.24	15
Airfoil type	NACA 0012	NACA 0015
Tip Mach no.	0.60	0.60
Pre-twist (deg)	-10	-10
Flap displacement (deg)	±4	±4

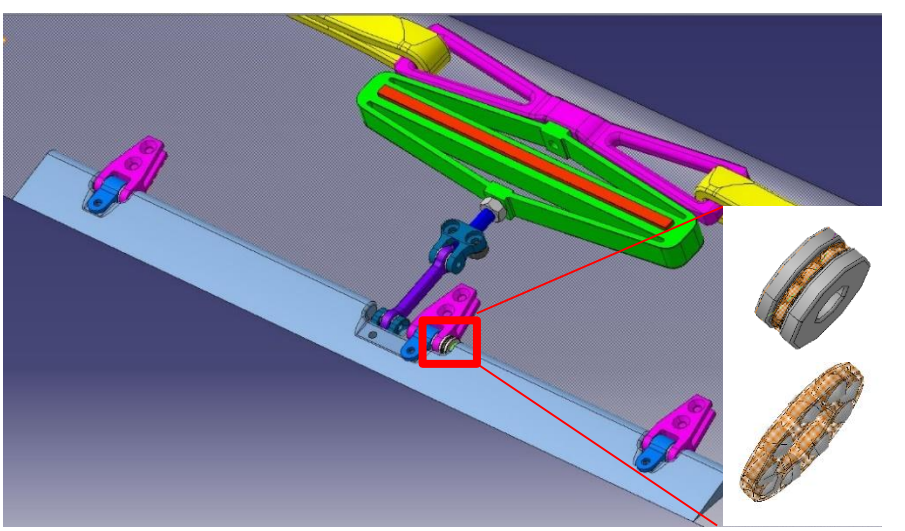

Figure 2.14 Thrust bearing (F3-8M)

2.6 Bench test of the revised test-bed

Non-rotating bench tests were carried out in order to validate the flap-driving mechanism. Preliminary preparation procedures for the non-rotating bench test are referred from the precedent thesis [10].

It is the Micro-Epsilon optoNCDT 1402-100 laser sensor which is the measurement equipment for the high frequency oscillations of the active flap. It enable us to figure out the displacement of the active flap angle. The following result as shown in Table 2.9 is obtained under the condition of at 10 Hz operating frequency.

Table 2. 9 Result of the bench test at 10 Hz operating frequency

Upper setting	7	deg
	0.1222	rad
	2.2101	mm
Hinge - laser	18	mm
Measured displacement	8.4239	mm
Lower displacement	6.2138	mm
	0.3324	rad
	19.045	deg

The actuation test at 10 Hz showed flap deflection about 20 degrees. It was more optimistic result than it had been expected. However, what remains to be fixed by further bench test is the flap fixing bolt of the flap hinge as depicted in Figure 2.15. It became loose and fell off at around 70 ~

80 Hz operating frequency during the tentative bench-test for selecting the appropriate amplifier. It should be gone over how to resolve this deficiency. Applying some kind of adhesives on it will be the most effective method so far, even though unpredicted frictions may occur.

On the other hand, a high voltage amplifier is needed, so as to operate the APA 1000L piezoelectric actuator at or above 65 Hz high frequency during the dynamic test. Active flap driving frequency was calculated as about 65 Hz. Therefore, the amplifier selection procedure was conducted to figure out the most appropriate amplifier model for the SNUF. The maximum operating frequency of each amplifier was estimated, according to Equation (5), and the results were depicted in Table 2.10.

$$f_{\max} \approx \frac{i_{\max}}{2CU_{P-P}} \tag{5}$$

$i_{\max}$ = Peak amplifier sourcesink current [A]

$f_{\max}$ = Maximum operating frequency [A]

C = Piezo actuator capacitance [Farad(As/V)]

$U_{P\text{-}P}$ = Peak to peak drive voltage [V]

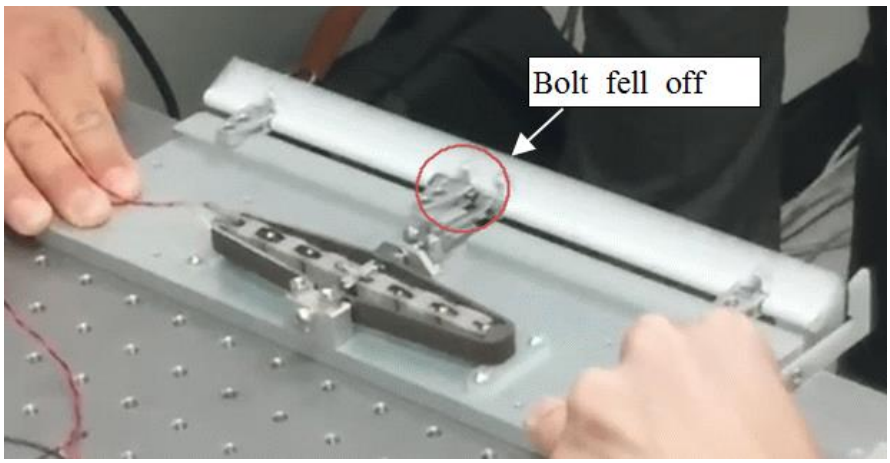

Figure 2.15 Bolt fell off phenomenon

Table 2.10 Comparison of the amplifiers possibly used

	Cedrat		Trek	NF
Amplifier product	SA75A	LA 75C	PZD 2000A	HAS 4052
$I_{max\ [A]}$	5 A	2.4 A	0.2 A	2 A
actuator capacitance [F(As/V)]	0.00004	0.00004	0.00004	0.00004
voltage[V]	140	140	140	140
F_{max}	446 Hz	214 Hz	17 Hz	178 Hz

The amplifier SA75A shows the best available operating frequency as it has the maximum output current. The amplifier will be selected after the validation of its application is completed.

III. Blade design and structural analysis

3.1 Blade design reconfigurations

The previous SNUF blade was the small-scale articulated type rotor blade based on the design of the existing SHARCS and NASA/ARMY/M.I.T. Active Twist Rotor (ATR) blades [10]. Table 3.1 shows the general properties of the ATR and SHARCS rotor blades [11]. However, the design based on both ATR and SHARCS blade properties imposed a constraint on selection of the actuator which brought about the complexities of the flap driving mechanism. In addition, ATR blade was designed to operate in a heavy gas environment which means the rotating RPM of ATR blade would become much lower than actual normal atmospheric testing condition of the SNUF.

Therefore, the blade revision process required many changes to overcome existing problems mentioned before. First critical change is that the number of the SNUF blade, reduced from 4 to 2. The rotating RPM of the SNUF should be increased, not like the ATR blade, in order to maintain the same tip Mach number. Thus, the SNUF blade RPM was selected as 1,298 RPM. If a 4 blade rotor needs 3/rev and 5 /rev to control the vibration, its maximum actuation frequency of the piezoelectric actuator is 108 Hz at 1,298 RPM. That value is quite challenging to achieve during the rotating condition. Thus, the number of SNUF blade was changed as 2 blades to reduce the burden of the actuation frequency of the actuator. The 3/rev is the maximum value, as a result, and it will need 65 Hz at 1,298 RPM. It is not likely to occur actuation problem if the SNUF operates within the criteria. Second important change is that the NACA 0015 airfoil is selected instead

of the NACA 0012, in order to accommodate the revised flap driving mechanism. Installing the revised flap driving mechanism required bigger inner space of the SNUF blade because of the newly selected APA 1000L actuator. It was inevitable measure to obtain the target flap deflection angle. The revised blade needed a new structural integrity analysis. This will be discussed later chapter. The last crucial change is that the built-in twist is now applied through the whole span-wise location without an exception on the actuation region. (Previously the active flap region was flat.) The previous blade design used partially linear built-in twist distribution along the blade span. The baseline built-in twist angle of the blade was -10°. The partial built-in twist ensued the structural integrity issues. Since fabrication of the mold for this partially built-in blade was tremendously challenging, the main issue would be how to connect the twisted region and untwisted region without any loss of structural integrity. Furthermore, the implementation of the built-in twist was difficult in the previous design due to the complexity of the flap driving mechanism with multiple relevant components such as fixed housing, etc. However, the APA 1000L actuator enabled the application of the built-in twist on the whole span of the blade by simplifying the actuation components. The built-in twist applied through the whole span-wise location is now expected to enhance the structural integrity, and gives aerodynamically-efficient rotor blade compared with the previous partially twisted blade. The profile view of the previous and the present blade designs are shown in Figure 3.1. Another revised properties are also shown in Table 3.2.

Table 3. 1 Properties of ATR and SHARCS rotor blades

	ATR	SHARCS
Control method	Active twist	Hybrid
Rotor radius (cm)	139.7	109.6
Rotation speed (rpm)	687.5	1,555
Blade chord (mm)	108	80
Airfoil type	NACA 0012	NACA 0015
Tip Mach number	0.603	0.52

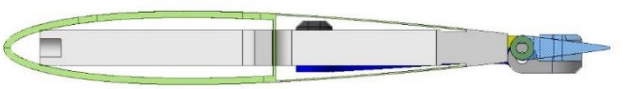

(a) The previous blade (Untwisted actuation region)

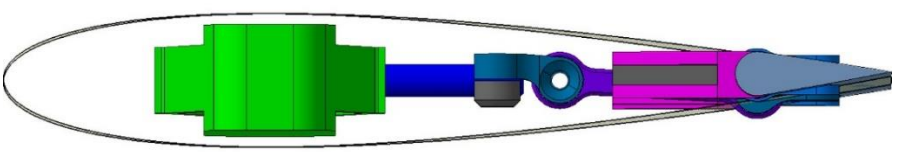

(b) The present blade (Twisted actuation region)

Figure 3.1 The profile view of the previous and the present blade design

Table 3. 2 The revised SNUF properties

Rotor type	Articulated	Teetering
Rotor radius, R (cm)	128	150
Rotation speed (rpm)	1,528 (160 rad/s)	1298 (135 rad/s)
Blade chord, c (cm)	10.24	13.5
N_b	4	2
Flap location	75% R	75% R
Flap length	20% R	20% R
Flap chord	15% R	15% R
Hinge offset(cm)	5.12	TBD
Flap Hinge offset(L_2) (mm)	0.9	TBD
Root cutout (% span)	20	20
Airfoil type	NACA0012	NACA 0015
Tip Mach number	0.60	0.60
Mass per unit length (kg/m)	0.55	1.0
Pre-twist (deg)	-10	-10
Flap displacement	±4˚	±4˚

3.2 Structural analysis for revised blade

3.2.1 Blade cross section design and analysis

The cross-sectional design was to be modified based upon the improved actuation mechanism, airfoil and increased chord length. The previous cross-sectional design had a spar located at 44.3 % of the chord. However, revised cross section design needs to eliminate the spar because the present actuation mechanism does not provide appropriate inner space. Thus, it was revised that the carbon composite materials are covered from leading edge to 14.8% of the chord. Figure 3.2 shows the previous cross sectional design and the current cross sectional design.

One of the characteristics of the revised cross sectional design is that the leading edge was filled with glass fiber roving. Another imperative characteristic of the revised cross section is shown in Figure 3.3. The titanium block was placed to hold the actuation part, and the titanium block is fixed by the glass fiber roving. Therefore, cross sectional analysis was conducted on two separate sections respectively consisting of a titanium block and composites. The cross-section properties of the present design are described in Table 3.3. All the stiffness values were increased compared with those of the previous cross-section. The detailed cross-sectional analysis was performed by using UM/VABS [16].

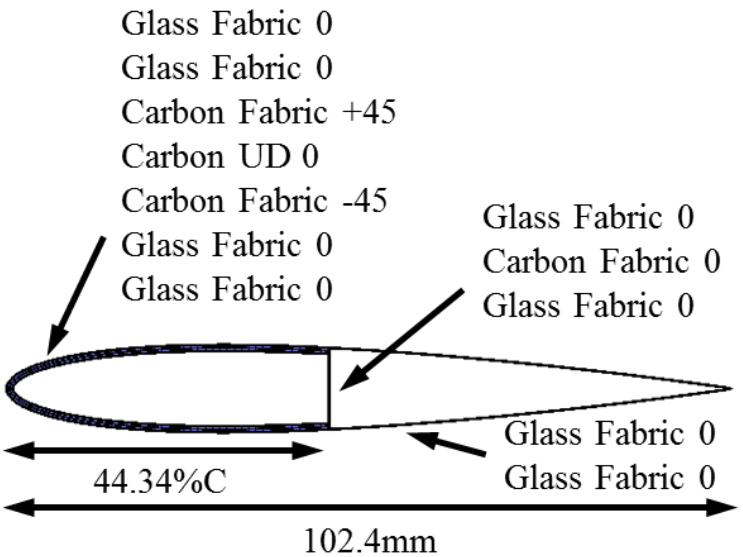

(a) The previous cross section design (NACA 0012)

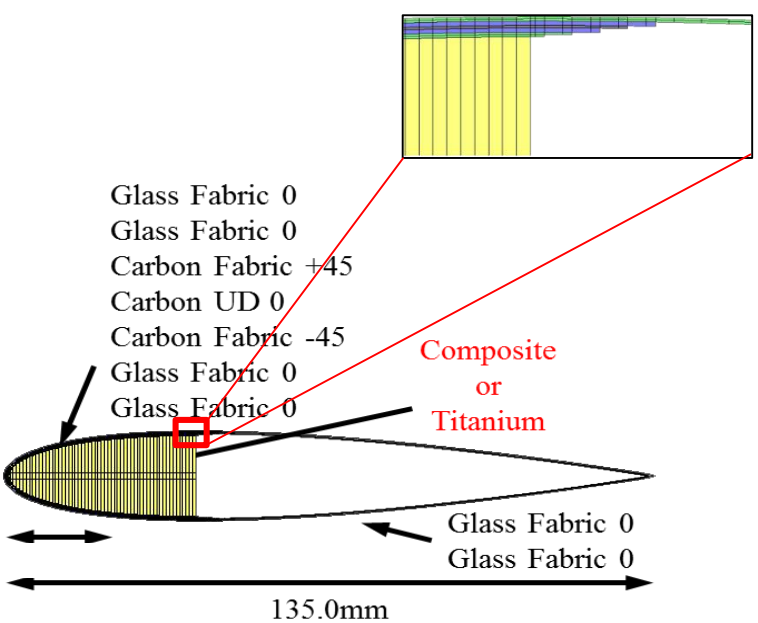

(b) The revised cross section design(NACA 0015)

Figure 3. 2 Comparison of the cross section designs

Table 3.3 Cross section analysis results

Properties	Previous	Present (Composite)	Present (Titanium)
EA (N)	3.628×10^{6}	7.034×10^{6}	5.014×10^{7}
GJ (N-m^2)	6.573×10^{1}	7.799×10^{1}	3.634×10^{2}
EI_{flap} (N-m^2)	7.864×10^{1}	1.801×10^{2}	4.397×10^{2}
EI_{lag} (N-m^2)	5.366×10^{3}	5.486×10^{3}	8.107×10^{3}
Mass per unit span (kg/m)	2.089×10^{-1}	4.928×10^{-1}	1.149×10^{0}

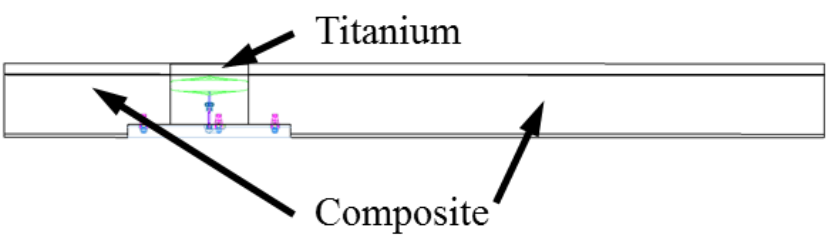

Figure 3. 3 Spanwise location of the cross section

3.2.2 Loads estimation

The internal forces and moments at each blade section was predicted by applying the CAMRAD II [17] for the forward flight condition with the advance ratio of 0.3. CAMRAD II is a comprehensive rotorcraft analysis program. CAMRAD II incorporates a combination of advanced technologies, including multi-body dynamics, nonlinear finite elements, and rotorcraft aerodynamics.

Two rotor blade condition was applied for revised blade internal load analysis instead of the previous four rotor blades as well the teetering hub blade was changed instead of the articulated rotor blade. In addition to the change, the whole rotor blade length was increased up to 1.5m in order to reduce the centrifugal force which induces the severe load on the blade. The rotor RPM is decreased from 160 rad/s to 137 rad/s so as to maintain the Mach number 0.6. For this reason, it is expected the reduced RPM lead to the decrease of the centrifugal force. Put otherwise, it enables to decrease the internal load of the actuator which is located at 0.75% of the rotor length.

The load analysis condition is depicted in Table 3.4 The revised SNUF blade's APA 1000L actuator mass is 163g. The mass of APA 1000L actuator is three times heavier than the total mass of the four APA 200M actuators because the APA 200M actuator mass is 16g. Thus, it needs to be considered when the internal load analysis is going on. For this reason, all the actuation region components such as the push rod, the actuator, the hinge, etc. were applied as point masses during the internal load analysis as shown in Figure 3.4. The mass and inertia of each actuation component was confirmed by the CATIA design information. The detailed internal load analysis results are shown in Figures 3.5 ~3.8.

Table 3. 4 The internal load analysis condition

Properties	Previous	Present
Rotor type	Articulated	Teetering
Rotor radius	1.28 m	1.50 m
Rotational speed	160 rad/s 1,528 RPM	135 rad/s 1,298 RPM
Blade chord	102.4 mm	135.0 mm
Root cutout	20%	20%
Airfoil	NACA0012	NACA0015
Tip Mach No.	0.60	0.60
Pre-twist	-10°	-10°
Advance ratio	0.3	0.3

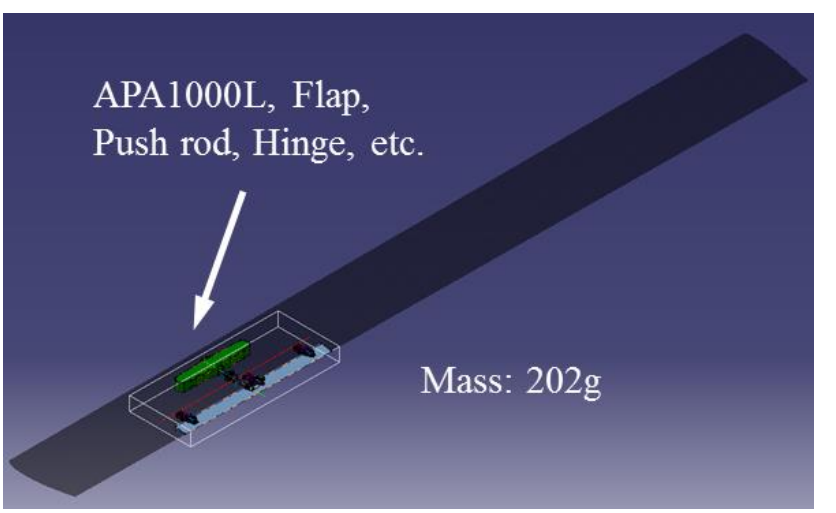

Figure 3. 4 Mass of the components included

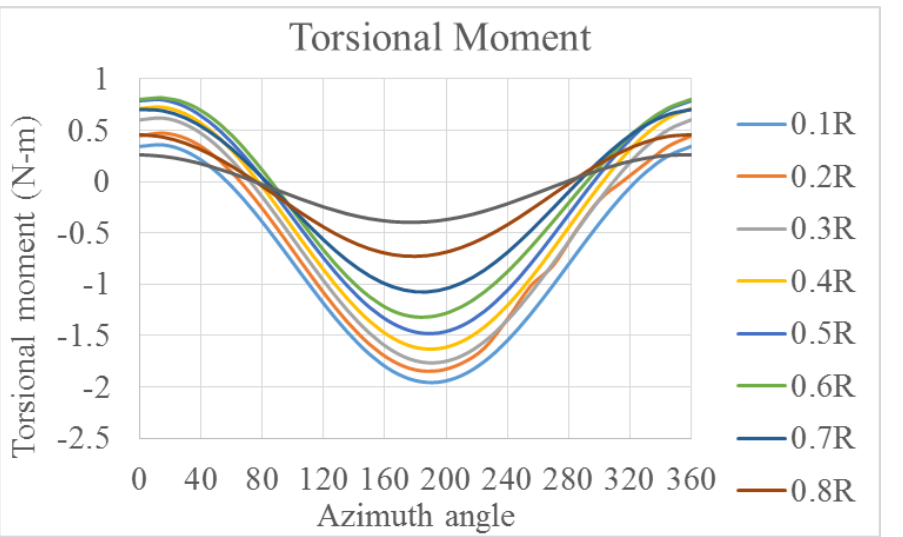

Figure 3. 5 Torsional moment distribution

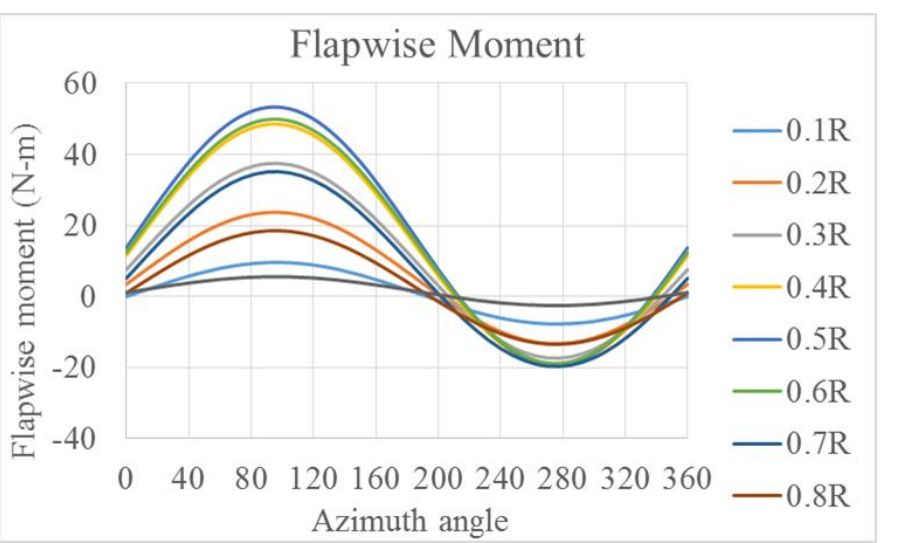

Figure 3. 6 Flapwise moment distribution

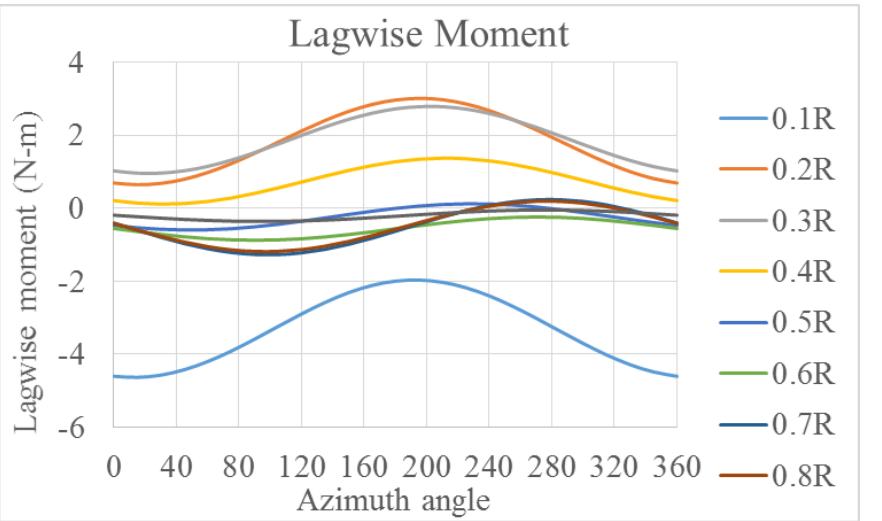

Figure 3. 7 Lagwise moment distribution

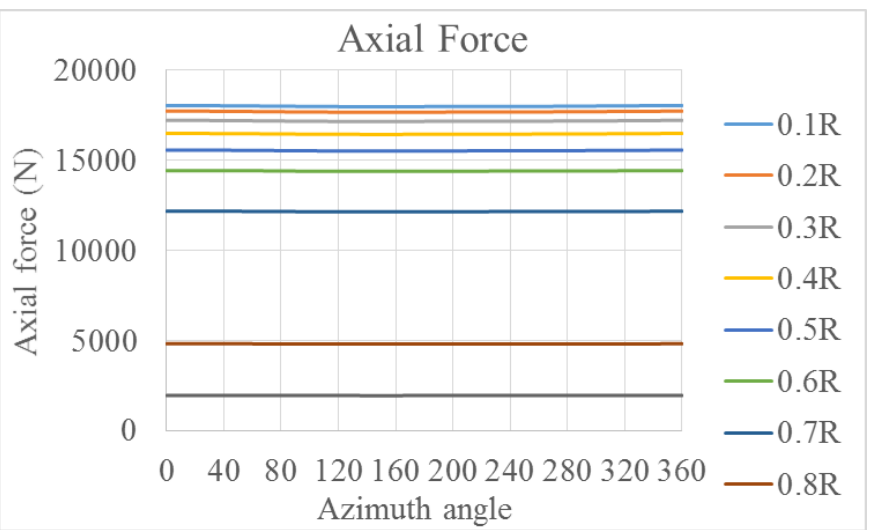

Figure 3. 8 Axial force distribution

3.2.3 Stress and strain recovery analysis

Stress and strain recovery analysis for the newly designed cross-section was conducted by utilizing the results of the internal load acting on the SNUF blade. This procedure was done to substantiate the structural integrity of the SNUF blade, and then a safety factor of 1.5 was considered in this structural integrity analysis. Internal load at the azimuth angle 90° was used.

Previous design using articulated hub has the maximum strain at the 30%R location. However, the maximum strain of the newly designed SNUF blade was observed at the load hub as shown in Figure 3.9. It seems reasonable that the revised SNUF blade uses the teetering rotor hub instead of the articulated rotor hub. No ply failures are occurred and maximum strains in all three directions are within the allowable strain levels as depicted in Table 3. 5.

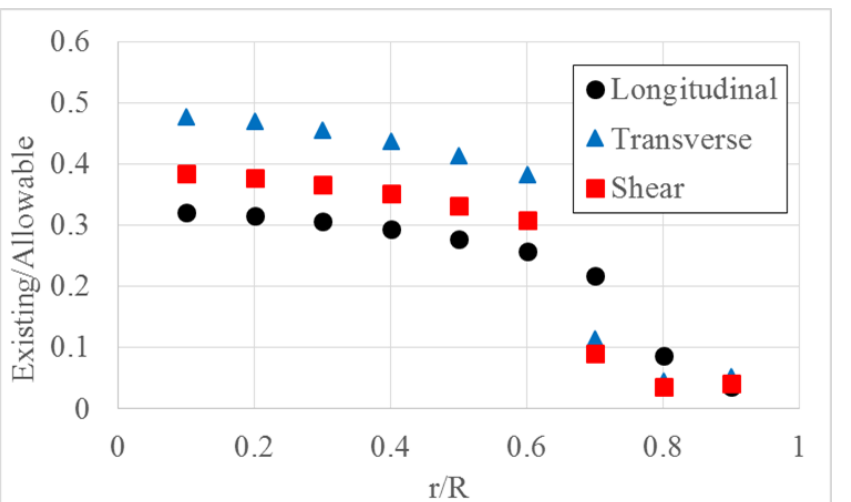

Figure 3.9 Strain distribution results

Table 3. 5 Maximum strain results

	Existing/Allowable		
	Longitudinal	Transverse	Shear
Previous	0.5387	0.3994	0.1812
Present	0.3205	0.4777	0.3837
Diff. (%)	+ 40.5	+ 19.6	+ 111.8

However, the present cross sectional design will be updated as the optimization process is conducted for better structural integrity, lighter blade weight, and for adjustment of the shear center. Figure 3.10 indicates the tentative cross section design filled with 10%c roving to reduce the SNUF blade weight. As a result, it ensued that two spars were needed to be installed to enforce the aerodynamic center located around 25%c. This cross section analysis was conducted in the way as mentioned above. However, it did not fall into acceptable strain level in terms of the longitudinal loads condition as shown in Table 3.6. Thus, it needs further improvement.

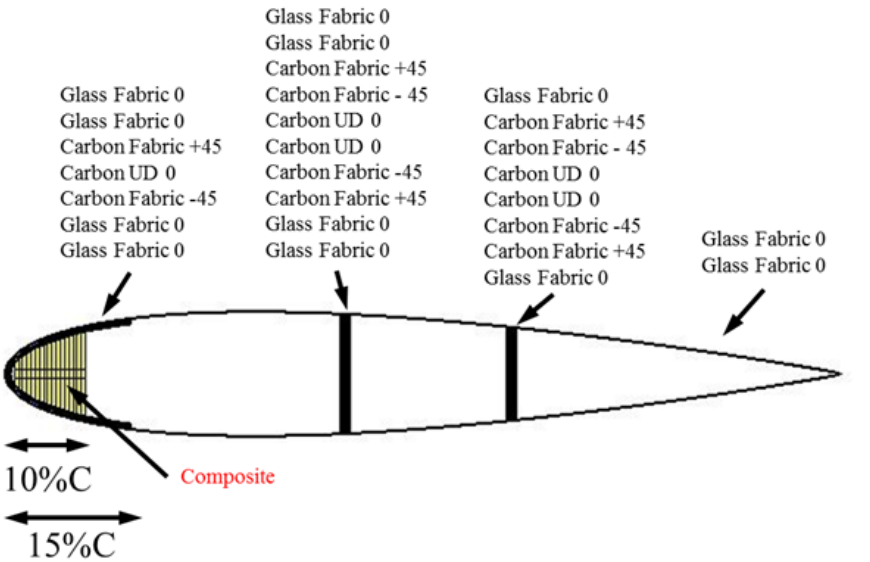

Figure 3.10 The cross section design filled with 10%C roving.

Table 3.6 Maximum strain results for the tentative cross section design

	Existing/Allowable		
	Longitudinal	Transverse	Shear
Tentative	104%	83%	82%

IV. Conclusion and future works

4.1 Conclusion

In this dissertation, the small-scaled blade prototypes with the flap-driving mechanism, called SNUF (Seoul National University Flap), were manufactured, and tested in order to realize vibratory load reduction in the rotor system. It was achieved by an active trailing-edge flap which is based on piezoelectric actuator. However, it turned out that the target value of the flap deflection angle was not accomplished in the previous designs. Therefore, the flap driving mechanism needs to be amended. Thus, a new piezoelectric actuator was selected to achieve the target deflection by considering the nonlinear relationship between flap deflection angle and the moment arm length, and by conducting the aerodynamic analysis of the active flap. Consequently, the APA 1000L actuator was finalized instead of the previous APA 200M actuator. Re-selection of the actuator required increase of the blade inner space and its size. Therefore, it was required to validate the cross-sectional design of the increased blade again. So as to verify the structural integrity, a cross-sectional analysis was conducted by using UM/VABS, and CAMRAD II. No ply failures are occurred and maximum strains in all three directions are within the allowable strain levels. However, it needs to be conducted again after the rotor blade hub design is determined.

The revised flap-driving mechanism showed the satisfactory results during the non-rotating static test. The current non- rotating test for the new flap driving mechanism achieved 20 degrees at 10Hz actuation condition. It seems no problem to obtain target deflection value($\pm 4^\circ$) during the

rotating test condition. Nonetheless, the bolt fell off phenomenon of the flap-driving mechanism should be amended during the high actuation frequency condition. It remains to be seen whether changing the flap-driving mechanism design or just putting adhesives on that.

After completion of the non-rotating static test of the new flap-driving mechanism, a prototype blade will be manufactured and tested in the whirl tower.

4.2 Future works

The current non-rotating bench test of the SNUF blade was conducted without direct consideration of centrifugal force acting on the active flap. Therefore, it is required to take the centrifugal force into consideration before carrying out the actual rotating test in order to validate the flap deflection angle about whether it shows a satisfactory result or not. This non-rotating bench test will be conducted with equivalent centrifugal force acting on the active flap.

For a conservative design, the current CFD FLUENT analysis process was conducted at 10° deflected condition in the light of the maximum aerodynamic pitching moment condition. In addition, the formula suggested by Lee was also carried out for comparison with CFD FLUENT results. As a result, CFD FLUENT analysis results were adopted because the CFD FLUENT analysis results were mostly 20% higher than that predicted by the formula by Lee. However, so as to achieve the more accurate hinge moment, precise prediction about aerodynamic analysis under transient condition needs to be executed by using ANSYS (CFD FLUENT)

The deflection of the SNUF was measured by the Micro-Epsilon

optoNCDT 1402-100 laser sensor. However, it is only available for the non-rotating test of SNUF blade, but not applicable for the rotating test. Therefore, a new measurement equipment is needed for the high frequency oscillation of the active flap during the rotating environment. Up to now, Hall effect sensors were considered to address this issue. It seems most feasible to figure out the flap displacement during the rotating condition. However, installation of Hall sensor may be difficult because of the limited space along the blade span. It needs more improvement on that.

Even though the present structural integrity of the SNUF blade provides allowable strain level, the present cross-sectional design will be further optimized considering the appropriate blade root design which is dependent on whirl tower facility. Currently, it is not determined yet which whirl tower facility will be used for the SNUF blade rotating test.

Manufacturing of the prototype of SNUF blade is scheduled after successful completion of non-rotating test for the test-bed. And then, active flap control algorithm design will be conducted to obtain the most effective vibration reduction result. In parallel, whirl tower test and validation for SNUF under the rotating situation will be carried out to figure out the flap-driving mechanism performance and vibration reduction capability.

Reference

[1] Chopra, I. and Datta, A., "Helicopter Dynamics", ENAE 633, Spring 2011, pp. 54-55.Johnson, W., *Helicopter Theory*, Chap. 12, Dover publications, Inc., N.Y., 1994.

[2] Lee, J. H., Natarajan, B., Eun, W. J., Viswamurthy, S. R., Park, J. S., Kim, T. S. and Shin, S. J., "Structural and Mechanism Design of an Active Trailing-edge Flap Blade", Journal of Mechanical Science and Technology, Vol. 27, No. 9, 2013, pp. 2605-2617.

[3] Pearson, J. T., Goodall, R. M. and Lyndon, I., "Active Control of Helicopter Vibration", Computing and Control Engineering Journal, Vol. 5, No. 6, 1994, pp. 277-284.

[4] Chiu, T., Friedmann, P. P., "ACSR system for vibration suppression in coupled helicopter rotor/flexible fuselage model", Technical Papers. Pt. 4(A96-26801 06-39), Reston, VA, American Institute of Aeronautics and Astronautics, 1996, p. 1972-1990.

[5] Patt, D., Liu, L., Chandrasekar, J., Bernstein, D. S., and Friedmann, P. P., "Higher-Harmonic-Control Algorithm for Helicopter Vibration Reduction Revisited", Journal Of Guidance, Control, And Dynamics, Vol. 28, No. 5, September–October 2005, PP.918-930.

[6] Kessler, C., "Active rotor control for helicopters: motivation and surveyon higher harmonic control", European Rotorcraft Forum 2010.

[7] Crozier, P., Leconte, P., Delrieux, Y., Gimonet, B., Le Pape, A., and des Rochettes, H.M., "Wind-Tunnel Tests of a Helicopter Rotor with Active Flaps", Proceedings of the 32nd European Rotorcraft Forum, Maastricht, The Netherlands, September 2006.

[8] Ahci, E., Rupert, P., Straße, W. M., "Structural Design, Optimization and Validation of the Integrated Active Trailing Edge for a Helicopter Rotor Blade", The American Helicopter Society 64th Annual Forum, Montreal, April 2008.

[9] Ahci-Ezgi, E., Pfaller, R., Denecke, U., Kuntze-Fechner, G., Muller, C.,

"Piezo Active Rotor Blade - Challenges and Solutions", The American Helicopter Society 69th Annual Forum, Phoenix, Arizona, May 21-23, 2013.

[10] Natarajan, B., "Structural Analysis and Actuation Tests of an Active Trailing-edge Flap (ATF) Blade for Helicopter Vibration Control 2013", Seoul National University, Master's Thesis, School of Mechanical and Aerospace Engineering, Seoul National University, Seoul, Korea (Rep. of), Feb. 2013.

[11] Lee, J., "Design of an Intelligent Active Trailing-edge Flap Rotor Blade for Decreased Vibration in Helicopter", Master's Thesis, School of Mechanical and Aerospace Engineering, Seoul National University, Seoul, Korea (Rep. of), Feb. 2011.

[12] Lee, T., and Chopra, I., "Design of Piezostack-driven Trailing-edge Flap Actuator for Helicopter Rotors", Smart Material and Structures, Volume 10, No 1, 2001, pp. 15-24.

[13] Shin, S. J., "Integral Twist Actuation of Helicopter Rotor Blades for Vibration Reduction", PhD Thesis, Aeronautics and Astronautics Dept., Massachusetts Institute of Technology, Cambridge, MA, USA, 2001.

[14] Feszty, D., Nitzsche, F., Khomutov, K., Lynch, B.K., Mander, A., and Ulker, F.D., "Design and Instrumentation of the SHARCS Scaled Rotor with Three Independent Control Systems", American Helicopter Society 64th Annual Forum, Montreal, Canada, Apr-May 2008.

[15] Mainz, H., van der Wall, B. G., Leconte, P., Ternoy, F., and Rochettes, H. M., "ABC Rotor Blades: Design, Manufacturing and Testing", 31th European Rotorcraft Forum, 2005, pp.118.1~118.15.

[16] Palacios, R. and Cesnik, C. E. S., "Cross-Sectional Analysis of Non-Homogeneous Anisotropic Active Slender Structures", AIAA Journal, Vol. 43, No. 12, 2005, pp. 2624-2638.

[17] Johnson, W. "Technology Drivers in the Development of CAMRAD II", American Helicopter Society Aeromechanics Specialist Meeting, San Francisco, CA, January, USA, 1994.

국문초록

본 연구에서는 압전재료 작동기(Piezoelectric actuator)에 기반한 지능형 뒷전 플랩의 고차조화제어를 통하여 로터 블레이드의 진동 하중 감소를 구현하기 위해 구동부 시제품을 제작/시험하였다. 하지만, 정적시험에서 이전 설계에서 선정된 APA 200M 작동기로는 목표 플랩 변위값(±4°)을 획득할 수 없었으며, 이에 본 논문에서는 정적시험 및 동적(회전)시험에서도 목표 플랩 변위값을 획득하기 위한 작동기 재선정 및 플랩 연결 메커니즘의 설계를 수정/보완하고자 하였다. 그래서, 목표플랩 변위값을 획득하기 위하여 플랩변위각과 모멘트팔 길이의 비선형적 관계를 고려하여 새로운 압전재료 작동기를 선정하였다. 하지만, 새롭게 선정된 압전재료 작동기는 블레이드 내부공간 및 크기증대가 수반되어, 블레이드 단면구조 설계를 재수행하였다. 단면구조 설계 및 구조적 강건도를 확인하기 위하여 UM/VABS을 사용하였다. 개선된 플랩구동부는 비록 해결해야 할 몇 가지 문제가 있지만, 비회전 정적시험에서 만족할만한 결과를 얻었다. 구동부의 비회전 정적시험 종료 후에는 블레이드 시제품을 제작할 예정이며, 휠타워 시험을 진행할 예정이다.

주요어: 지능형 능동 뒷전 플랩(ATF), 압전재료 작동기, 진동제어, 지능형 로터 블레이드

학번 : 2013-22481